Supporting Information

Schuster et al. 10.1073/pnas.1015839108

SI Methods

Strains. The *Ustilago maydis* strains AB33ΔKin3, AB33G_3Dyn2, FB1Dyn2^{ts}, and FB2N107G_ER were described previously (1, 2). Strain AB33nRFP, which expresses red fluorescent protein fused to the nuclear localization signal of the GAL-4 DNA binding domain from pC-ACT1 (Clontech), was generated by ectopic integration of plasmid poNLS3RFP in strain AB33. For studies of moving EEs an ectopic fusion of photoactivatable GFP (3) (kindly provided by J. Lippincott-Schwartz, Eunice Kennedy Shriver National Institute of Child Health and Human Development, Bethesda, MD) to the endosome-specific Rab5a (4) under the control of the constitutive *otef* promoter (5) was generated and integrated into the succinate dehydrogenase locus (6) or ectopically in the genome of strains AB33, AB33ΔKin3, and AB5Dyn2^{ts}, resulting in strains AB33paGRab5a, AB33ΔKin3_paGRab5a, and AB5Dyn2^{ts}_paGRab5a. To analyze turning events of EEs, strain AB33Dyn2Ch_3_paGRab5a was generated by transforming plasmid pDyn2_3Ch in strain AB33paGRab5a. For strain AB33Δ-Kin3_Kin3G_ChRab5a the *kin3* gene in strain AB33 was deleted. After confirming deletion by Southern blot analyses, the plasmids pKin3G and po$_m$ChRab5a were introduced. For colocalization studies of dynein and EEs strain AB33G_3Dyn2_ChRab5a was generated by introducing the plasmid po$_m$ChRab5a in strain AB33G_3Dyn2. To study the run length of dynein, the plasmid pPaGFP$_3$Dyn2 was transformed into AB33, resulting in strain AB33paG_3Dyn2. The genotypes of all strains are summarized in Table S2.

Plasmid Construction. ***poNLS3RFP.*** Plasmid poNLS3RFP was generated by using the plasmid pH_NLS3 _ RFP (7) to replace the hygromycin resistance cassette with the nourseothricin resistance cassette. For this process the plasmid was digested with SnaBI and HindIII to obtain a 6,644-bp fragment containing the constitutive *otef* promoter, the nuclear localization signal of the GAL-4 DNA binding domain from pC-ACT1 (Clontech), a triple-RFP tag, the T_{nos} terminator, and the ampicillin resistance cassette. The nourseothricin resistance cassette (1,609 bp) was obtained by digesting the cloning vector pSL-Nat with SnaBI and HindIII.

popaGRab5a. Plasmid popaGRab5a was constructed as follows: A 708-bp fragment (cut by NcoI and NdeI) containing the photoactivatable GFP (3) was cloned into plasmid p123 (8), downstream of the constitutive *otef* promoter, resulting in plasmid p123-paGFP. The full-length *rab5a* gene (4) and its terminator sequence were amplified by PCR, cut by NdeI and EcoRI, and subsequently fused in frame with paGFP in plasmid p123-paGFP, cut by the same restriction enzymes, generating an N-terminal fusion. The resulting plasmid was linearized with SspI before fungal transformation to direct its homologous integration at the *sdh2* succinate dehydrogenase locus.

pDyn2_3$_m$Ch. To generate plasmid pDyn2_3$_m$Ch a cloning plasmid containing single *mCherry* was used to create the triple tandem repeat tag. The complete tag was amplified by a second PCR, using primers that generated NcoI and NotI restriction sites to each end. The obtained 2,176-bp DNA fragment was digested with NotI, and the resulting 2,169-bp fragment was cloned in front of the T_{nos} terminator. After digestion with NcoI and BglII, the resulting 2,471-bp fragment was cloned downstream of a 1,555-bp (HindIII, NcoI) fragment of the 3′ end of *dyn2* and then a 1,427-bp fragment (SacII, BglII), containing the nourseothricin resistance cassette, and a 672-bp fragment (SacII, EcoRI), containing part of the dynein terminator sequence, were added downstream of the T_{nos} terminator to trigger homologous recombination. A pNEB193 vector (New England Biolabs) was digested with HindIII and EcoRI. The resulting 2,635-bp fragment, containing the ampicillin resistance cassette and the *Escherichia coli* origin of replication, was used as a backbone for the resulting vector. For homologous integration in the native *dyn2* locus the plasmid was digested with DraI and HindIII.

pΔKin3. To obtain the plasmid pΔKin3 a 980-bp fragment containing part of the *kin3* promoter and a 1,075-bp fragment containing downstream sequence of the *kin3* gene were amplified be PCR. The promoter flank was digested with NotI and KpnI and the terminator flank with NotI and SphI. Both fragments were cloned in the pTZ 19 R vector (Fermentas), which was digested with KpnI and SphI. The resulting plasmid was cut with NotI and the nourseothricin resistance cassette (cut by NotI) was cloned between the two flanks. For transformation into *U. maydis* the plasmid was digested with KpnI and SphI.

po$_m$ChRab5a. The plasmid po$_m$ChRab5a was generated by cloning a 723-bp fragment (cut by NcoI and NdeI) containing the mCherry gene downstream of the constitutive *otef* promoter carried by plasmid p123. The mCherry gene was then N-terminally fused to the full-length *rab5a* followed by its terminator, obtained as described above. The nourseothricin resistance cassette (cut by NotI) was cloned upstream of the *otef* promoter. The resulting plasmid was linearized with SapI before fungal transformation, leading to ectopic integration in the genome.

pPaGFP$_3$Dyn2. For generating plasmid pPaGFP$_3$Dyn2 a plasmid containing single photoactivatable GFP was used as a template for generating the triple tandem repeat tag. In a first step the paGFP gene was amplified from the obtained vector. After blunt-end ligation of three paGFP amplicons, the complete triple tandem tag was amplified in a second PCR using primers that added NcoI and NdeI restriction sights to each end. The obtained 2,176-bp DNA fragment was digested with NcoI and NdeI, and the resulting 2,166-bp fragment was cloned downstream of a 1,724-bp fragment of the endogenous promoter of dyn2 followed by the first 1,762-bp of the coding sequence of *dyn2*, using NdeI and EcoRI restriction sites. The hygromycin phosphotransferease resistance cassette and a 1,261-bp fragment of the dyn2 promoter were added upstream of the dyn2 promoter to trigger homologous recombination. The plasmid was digested with SphI and EcoRV for homologous integration in the native *dyn2* locus of strain AB33, resulting in AB33paG3Dyn2 (Table S2).

Microscopy and Image Analysis. Cells were placed on a thin layer of 2% agarose in water and observed using an IX81 microscope (Olympus), equipped with a 100×/1.45 Oil TIRF objective and a VS-LMS4 Laser-Merge System with solid state lasers (488 nm/70 mW and 561 nm/70 mW; Visitron System). Photoactivation and photobleaching experiments were performed using a 405 nm/60 mW diode laser. Colocalization was performed using a Dual-View Microimager (Photometrics) and appropriate filters. Images were captured using a Photometrics CoolSNAP HQ2 camera (Roper Scientific). The system was controlled by MetaMorph (Molecular Devices). Fluorescence measurements and image processing were carried out with MetaMorph, and statistical analysis was done using Prism4 (GraphPad).

Activation of Photoactivatable Rab5a and Photoactivatable Dynein. Strains AB33Dyn2Ch_3_paGRab5a, AB33paGRab5a, AB33ΔKin3_paGRab5a, AB5Dyn2ts_paGRab5a, and AB33paG_3Dyn2 were shifted to hyphal growth and were placed on a 2% agar cushion.

To visualize the photoactivatable GFP, a 25-ms laser pulse (2% output power of a 60-mW, 405-nm laser) was used, followed by immediate observation using the 488-nm/70-mW laser at 15% output power.

Visualization of Fluorescent Motor Proteins. Motors were visualized in hyphae of strains AB33G$_3$Dyn2, AB33G$_3$Dyn2_ChRab5a, and AB33ΔKin3_Kin3G_ChRab5a (Table S2). A region of 10 μm in length at 5 μm behind the tip was radiated for 150 ms with a beam diameter of 30 pixels using 22.5% output power of a solid-state 60-mW, 405-nm laser. To visualize the loading and offloading process of EE onto dynein a 20-μm region 5 μm behind the tip and a second 20-μm region near the center of the cell were radiated for 150 ms with a beam diameter of 30 pixels using 22.5% output power of a solid-state 60-mW, 405-nm laser. This procedure was followed by observation using an exposure time of 50 or 150 ms and the 75-mW, 488-nm laser at 100% for dynein and kinesin-3. Seventy-five to 150 frames were taken for each experiment. Velocity, frequency, and turning rates were analyzed in kymographs that were generated from these image series using MetaMorph.

CCCP Influence on Signal Intensity. Cells expressing Kin3-GFP and GFP$_3$-Dyn2 were shifted to hyphal growth overnight and were treated with 100 μM carbonyl cyanide m-chlorophenyl-hydrazone (CCCP) (Sigma-Aldrich). After the majority of signals were immobilized (dynein, 15 min; kinesin-3, 5 min), images were taken immediately and after 4, 8, and 12 min. The integrated intensity was measured using MetaMorph and corrected for the cytoplasmic background.

Quantitative Photobleaching. Cells expressing Kin3-GFP and G3-Dyn2 were shifted to hyphal growth overnight. Strain AB33G$_3$-Dyn2 was treated with 100 μM CCCP for 10 min. After placing them on a layer of 2% agarose/100 μM CCCP the apical or subapical part of the whole hypha was photobleached using a 405-nm laser at 15 mW output power. After 5 min incubation in the dark, image series of 200 frames at 250 ms at 5.6-mW, 488-nm laser power were acquired. Kinesin-3–GFP was immobilized by treating the cells with 0.1% formaldehyde for 5 min. Average intensity of immobile signals was background corrected and imported in MatLab (MathWorks), and the number of bleaching steps was determined by a step-find algorithm (35) kindly provided by Jacob Kerssemakers, Delft, the Netherlands. For measurement of signal reduction per bleaching step the smallest signal decrease per frame interval and bleaching curve was selected from the numerical values recorded. The mean value of signal reduction per single GFP and Fig. 3*B* were derived from these data.

Quantitative Analysis of Fluorescent Intensities. Comparison of GFP$_3$-Dyn2 and Kin3-GFP with the nucleoporin Nup107-GFP as internal calibration standard was done as described (9). In brief, signals were immobilized (see above). Immobile signals were measured and corrected for the adjacent cytoplasmic background. A strain that expresses a fusion protein of the endogenous nuclear porin Nup107 and GFP was treated with CCCP and intensity of single pores was measured. For this quantitative analysis average or integrated signal intensities were corrected for the adjacent cellular background by copying the region of interest next to the signal that was not influenced by other fluorescent signals. The intensity of this region was subtracted from the measured signal intensity. Nup107-GFP is found in the pore 16 times, which allowed an estimation of the intensity of a single GFP in the living cell. This value was used to calculate the number of motors, given that each kinesin dimer contains two GFPs, whereas dynein dimers comprise six GFPs.

Mathematical Modeling. ***Model for dynein loading "on the run."*** The dynein loading on-the-run model addresses the question: What is the probability that an EE walking on a MT toward the tip meets a free retrograde walking dynein motor, loads onto dynein, and changes direction from anterograde to retrograde? To analyze this, we divided this process into two parts: First, we analyzed the "first-passage process" between EE and dyneins by calculating explicitly the trapping probability P_{trap} (i.e., the spatially dependent probability that an EE meets dynein). Then, we found an effective probability P_{load} for the loading process once an EE and a dynein meet. Our calculated P_{load} is consistent with the dynein-loading process in the hyphal tip (9). The turning probability is then given by $P_{\text{turn}} = P_{\text{trap}} \times P_{\text{load}}$. In this model we neglect effects arising from unbinding of kinesin-3 from MT due to Eq. **S4** and the number of kinesin-3 motors.

An important quantity in the first-passage process between EE and dynein is the density of free dyneins, ρ_{dynein}. Because this quantity is hard to determine experimentally, we chose a more microscopic approach in describing the system. In doing so we followed the time evolution of all motors. Every dynein starts its retrograde walk at the hyphal tip in the apical loading zone (at $x = L$). Its trajectory is given by

$$y_i(t,\tau_i) = -v\cdot(t-\tau_i)+L \equiv -v\cdot t+L+y_i^0(\tau_i). \qquad \textbf{[S1]}$$

Every EE starts at the nucleus (at $x = 0$) with trajectory $z_i(t) = v\cdot t$. In this description, the first-passage point is determined by the release time τ_i, i.e., EE and dynein meet at $x_1 = L/2 + y_1^0(\tau_1)$. If the EE does not load onto dynein, it keeps walking until it meets another dynein at $x_2 = L/2 + y_2^0(\tau_2)$ and so on. Because no information is available about the dynein density and the release time τ_i, we set $x_2 \equiv x_1 + \Delta_2$, $x_3 \equiv x_2 + \Delta_3$, ..., and we assume that x_1 and all Δ_i are Gaussian-distributed random variables with mean $\langle x_1\rangle, \langle\Delta\rangle$ and SDs $\sigma_{x_1}, \sigma_\Delta$. Thus, the mth possible turning point is given by a sum of Gaussian-distributed random distances

$$x_m = x_1 + \sum_{i=2}^{m}\Delta_i. \qquad \textbf{[S2]}$$

If the EEs reach one of these points, they load onto dynein with probability P_{load} and change direction from anterograde to retrograde. This "loading onto dynein" probability was chosen in such a way that it is consistent with the loading process in the apical loading zone at the hyphal tip that has been experimentally determined to be $P_{\text{load}} = 0.05$ (see below).

To compare the predictions of the model with the experimental findings we calculated the number of first turns as a function of distance to the hyphal tip. In doing so we set $\langle x_1\rangle = 900$ steps, $\sigma_{x_1} = 450$ steps, $\langle\Delta\rangle = 200$ steps, and $\sigma_\Delta = 100$ steps, where $x = 0$ steps is at the nucleus and $x = 5{,}000$ steps is at the hyphal tip. The results obtained from these parameter values are in excellent agreement with the experimental findings: The simulations yield a turning number 65 ± 1% (of 100,000 EEs) whereas experimentally 66.4% was obtained. A histogram of the simulated turning points is nearly identical to the experimental data (Fig. S5*A*) with a correlation coefficient of $r = 0.72$. This result suggests that the dynein "loading on the run" model is a very likely scenario for the first change in direction of the EE. It is worth noting that the above assumption that the motors start at the tip is not essential. The presented results are not affected if motors are recruited from the cytoplasm rather than being released from an apical dynein comet, as suggested by previous work (1, 9).

Dynein density. From the simulations we calculated an effective dynein density $\rho_{\text{dynein}}(x)$ as a function of distance x to the tip by averaging Eq. **S2** over 100,000 realizations. Because of the assumed Gaussian distributions, the density increases with decreasing distance to the tip. At a distance of ~30% (of total length) the density saturates at a value of 0.625 dynein/μm, i.e., 2.5 dyneins per 5% histogram interval (Fig. S5*B*). Integrating

over the whole interval ranging from nucleus to tip (40 μm), we get an average dynein number of 21.1, corresponding to an average dynein density of 0.53 dynein/μm.

Model for an apical loading zone. To estimate P_{load} we modeled the behavior of dynein at the apical comet, for which detailed data about dynein concentration and turning of EEs were available (9). For this system, the only difference is that dyneins have velocity zero and are linearly distributed over the whole loading zone. Experimental measurements have shown that the core dynein comet is ~640 nm in length (9), which equals 80 steps of 8 nm, the preferred step size of dynein (10). A theoretical analysis of the experimental apical loading zone data has revealed that 30–35 of a total of 61 dyneins per zone are involved in the loading process (9). Because the dynein density $\rho_{\mathrm{dynein}}(x)$ is proportional to the trapping probability $P_{\mathrm{trap}}(x)$, one immediately obtains

$$P_{\mathrm{trap}}(x) = \begin{cases} 0.175 & \text{for } 0 \le x \le 30 \\ 0.0165 \cdot x - 0.32 & \text{for } 30 \le x \le 80, \end{cases} \quad \textbf{[S3]}$$

where x is measured in steps; i.e., $x = 80$ at the hyphal tip (here $x = 0$ is the beginning of the apical loading zone and not the position of the nucleus). The trapping probability $P_{\mathrm{trap}}(x)$ is shown in Fig. S5*C*. Using this trapping probability we found for $P_{\mathrm{load}} = 0.05$ that $84 \pm 1\%$ of EEs that started at $x = 0$ turn before they reach the MT ends in agreement with the experimental results (Fig. S5*D*).

Theoretical estimation of run length of kinesin-3–driven endosomes. In the following we consider EEs that are transported by N active motors of a single species. For the scenario considered here these motors are kinesin-3. Nevertheless, our analysis is rather general and is applicable to other types of plus- or minus-end MT motors. Each single motor is irreversibly attached to the EE and walks along a MT with step size $\Delta x = 8$ nm and velocity $v = 1.5$ μm/s. They detach from the MT with probability P_{det} and (re)attach to the MT with probability P_{att}. If all N motors are detached from the MT, the EEs diffuse freely in solution with diffusion constant $D_{\mathrm{EE}} = 2 \times 10^{-3} \mu\mathrm{m}^2/\mathrm{s}$. The MT-motor system can be modeled as a one-dimensional lattice of length $L = 40$ μm = 5,000 motor steps (distance from the nucleus to the hyphal tip) and lattice constant $\Delta x = 8$ nm. The average walking distance $\langle \Delta x_{\mathrm{b}} \rangle$ of the EE transported by N motors in one direction on such a MT track (given by the average distance at which all motors are detached) obeys

$$\langle \Delta x_{\mathrm{b}} \rangle = \frac{v}{N P_{\mathrm{att}}} \left[\left(1 + \frac{P_{\mathrm{att}}}{P_{\mathrm{det}}} \right)^{N} - 1 \right]. \quad \textbf{[S4]}$$

This result implies that a larger number of bound motors leads to a larger average walking distance of EEs in one direction. With published parameter values [$P_{\mathrm{det}} = 1/187.5$ (11); $P_{\mathrm{att}} = 5/187.5$ (11); $P_{\mathrm{new}} = 0.5$; $v = 1.5$ μm/s; $\Delta x = 8$ nm (10)], we get $\langle \Delta x_{\mathrm{b}} \rangle = 1.5$ μm, 5.25 μm, 21.5 μm, and 97.125 μm for one, two, three, and four kinesin-3 motors, respectively.

1. Lenz JH, Schuchardt I, Straube A, Steinberg G (2006) A dynein loading zone for retrograde endosome motility at microtubule plus-ends. *EMBO J* 25:2275–2286.
2. Theisen U, Straube A, Steinberg G (2008) Dynamic rearrangement of nucleoporins during fungal "open" mitosis. *Mol Biol Cell* 19:1230–1240.
3. Patterson GH, Lippincott-Schwartz J (2002) A photoactivatable GFP for selective photolabeling of proteins and cells. *Science* 297:1873–1877.
4. Fuchs U, Hause G, Schuchardt I, Steinberg G (2006) Endocytosis is essential for pathogenic development in the corn smut fungus *Ustilago maydis*. *Plant Cell* 18:2066–2081.
5. Spellig T, Bottin A, Kahmann R (1996) Green fluorescent protein (GFP) as a new vital marker in the phytopathogenic fungus *Ustilago maydis*. *Mol Gen Genet* 252:503–509.
6. Loubradou G, Brachmann A, Feldbrügge M, Kahmann R (2001) A homologue of the transcriptional repressor Ssn6p antagonizes cAMP signalling in *Ustilago maydis*. *Mol Microbiol* 40:719–730.
7. Straube A, Weber I, Steinberg G (2005) A novel mechanism of nuclear envelope break-down in a fungus: Nuclear migration strips off the envelope. *EMBO J* 24: 1674–1685.
8. Aichinger C, et al. (2003) Identification of plant-regulated genes in *Ustilago maydis* by enhancer-trapping mutagenesis. *Mol Genet Genomics* 270:303–314.
9. Schuster M, et al. (2011) Controlled and stochastic retention concentrates dynein at microtubule ends to keep endosomes on track. *EMBO J*, 10.1038/emboj.2010.360.
10. Gennerich A, Carter AP, Reck-Peterson SL, Vale RD (2007) Force-induced bidirectional stepping of cytoplasmic dynein. *Cell* 131:952–965.
11. Müller JI, Klumpp S, Lipowsky R (2008) Motility states of molecular motors engaged in stochastic tug-of-war. *J Stat Phys* 133:1059–1081.

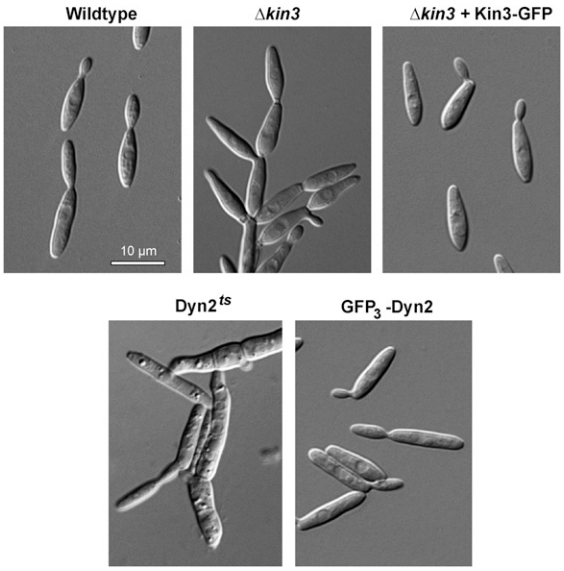

Fig. S1. Morphological phenotype of wild-type cells (wild type), kinesin-3 null mutants (Δ*kin3*), kinesin-3 null mutants that were rescued with a kinesin-3–GFP fusion protein (Δ*kin3* + Kin3-GFP), a temperature-sensitive dynein mutant (Dyn2^{ts}), and mutant cells that express a 3× GFP–dynein heavy chain fusion protein (GFP_3-Dyn2). Note that cells expressing GFP fusions to kinesin-3 and dynein show wild-type-like phenotypes.

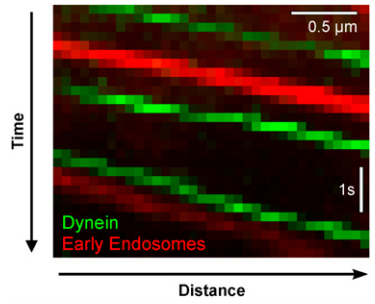

Fig. S2. Dynein and anterograde EEs. Dynein (green) does not colocalize with mCherry-Rab5a labeled EEs (red).

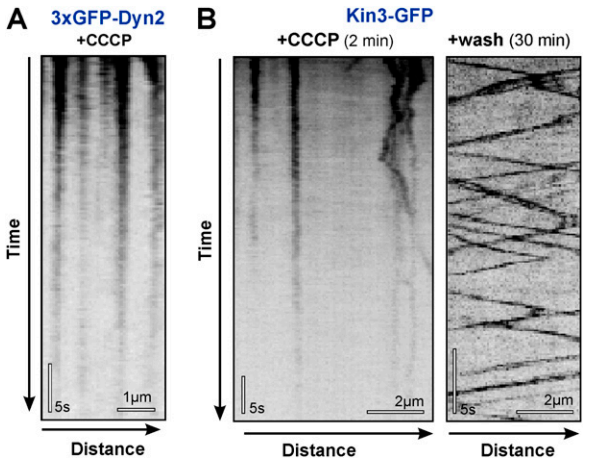

Fig. S3. Immobilization of Kin3-GFP and GFP_3-Dyn2 in living cells. (*A*) Kymographs showing inhibition of GFP_3-Dyn2 motility in cells treated with 100 µM CCCP for 15 min. Note that the motility can also be fully restored after washing the cells with fresh medium. (*B*) Kymograph of Kin3-GFP motility in cells treated with 100 µM CCCP for 2 min. Only few signals show motility. Motility is fully restored after washing the cells with fresh medium (wash out).

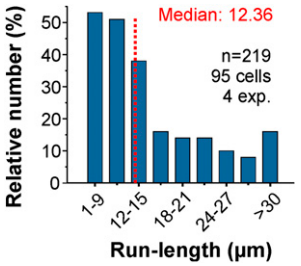

Fig. S4. Run length of paGFP3-Dyn2 signals activated in the hyphal apex. Note that due to signal interferences short runs (<10 µm) were difficult to access and are therefore underrepresented.

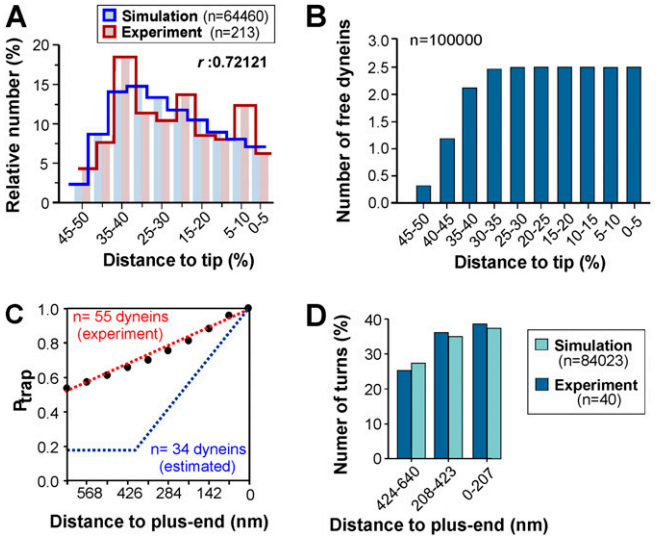

Fig. S5. Modeling the "on-the-run" loading. (*A*) Mathematical simulation of anterograde-to-retrograde turning events relative to the cell length for a dynamic on-the-run loading model. A correlation was found between the predicted distribution (blue) and the experimental data (red) (Spearman correlation coefficient is denoted by *r*). (*B*) Graph showing the effective number of dyneins as a function of distance to tip for the loading on-the-run model (see text for the parameters). The sum is equal to 21.1 dyneins distributed over the whole distance of 5,000 steps, which corresponds to an average of accessible (binding-competent) motors of 0.53 dynein/μm. (*C*) Graph showing the experimental measured dynein concentration (black dots, red curve) (9) in the apical comet in units of P_{trap} (the maximum of dynein density is at the hyphal tip where we set P_{trap}= 1). A theoretical analysis of the experimental apical loading zone data revealed that ∼30 of a total of 55 dyneins are involved in a stochastic loading process. Because the dynein density is proportional to the trapping probability $P_{trap}(x)$, one obtains the blue curve (Eq. S3). (*D*) Bar chart showing the number of turns of EEs in the dynein comet at the end of MTs. Experimental data were taken from ref. 9 and the simulation was adjusted so that it best fitted the observed experimental results. From this the P_{load} was derived for further simulations in the "on-the-run" loading model.

Table S1. Parameters of early endosome motility

	Anterograde*	Retrograde*	Different?
Velocity (μm/s)	2.30 ± 0.46 (103)	2.11 ± 0.43 (103)	Yes‖
Flux (events/s)†	0.82 ± 0.32 (79)	0.84 ± 0.31 (87)	No
Run length (μm)‡	22.22 (301)	23.32 (289)	No
Pausing (s)§	1.27 ± 1.75 (102)	1.00 ± 1.07 (76)	No
Immobile (%)¶		9.2 (120)	

*Mean ± SD (sample size).
†Taken ∼5 μm behind the cell tip.
‡Median; Mann–Whitney test; mean ± SD: 27.96 ± 20.91/ 29.36 ± 20.65.
§Before changing direction.
¶Mean number of EEs per cell without directed motility for >20 s.
‖Student's *t* test, P = 0.003.

Table S2. Strains and plasmids used in this study

AB33nRFP	*a2* P*narbW2* P*narbE1*, *ble*^{R}/poNLS3RFP	This study
AB33paGRab5a	*a2* P*narbW2* P*narbE1*, *ble*^{R}/popaGRab5a	This study
AB33Dyn2Ch$_3$_paGRab5a	*a2* P*narbW2* P*narbE1*, P*dyn2-dyn2-3x mcherry*, *ble*^{R}, *nat*^{R}/popaGRab5a	This study
AB33ΔKin3_paGRab5a	*a2* P*narbW2* P*narbE1*, Δ*kin3*, *ble*^{R}/popaGRab5a	This study
AB5Dyn2^{ts}_paGRab5a	*a1* P*nar-bW2* P*nar-bE1*, P*dyn2-dyn2*^{ts}, *ble*^{R}, *hyg*^{R}/popaGRab5a	This study
AB33ΔKin3_Kin3G_ ChRab5a	*a2* P*narbW2* P*narbE1*, Δ*kin3*, *ble*^{R}, *hyg*^{R}/pKin3G/po$_m$ChRab5a	This study
AB33ΔKin3_	*a2* P*narbW2* P*narbE1*, Δ*kin3*, *ble*^{R}, *hyg*^{R}	(1)
AB33G$_3$Dyn2	*a2* P*nar-bW2* P*nar-bE1*, P*dyn2-3xegfp-dyn2*, *ble*^{R}, *hyg*^{R}	(2)
FB1Dyn2^{ts}	*a1b,1* P*dyn2-dyn2*^{ts}, *nat*^{R}	(3)
AB33G$_3$Dyn2_ ChRab5a	*a2* P*nar-bW2* P*nar-bE1*, P*dyn2-3xegfp-dyn2*, *ble*^{R}, *hyg*^{R}/po$_m$ChRab5a	This study
FB2N107G_ER	*a2b2* P*nup107-nup107-egfp*, *ble*^{R}/pERRFP	(4)
AB33paG$_3$Dyn2	*a2* P*nar-bW2* P*nar-bE1*, P*dyn2-3xpagfp-dyn2*, *ble*^{R}, *hyg*^{R}	This study
poNLS3RFP	P*otef-gal4s-mrfp-mrfp-mrfp*, *nat*^{R}	This study
popaGRab5a	P*otef-pagfp-rab5a*, *cbx*^{R}	This study
pKin3G	P*kin3-kin3-gfp*, *cbx*^{R}	(5)
po$_m$ChRab5a	P*otef-mcherry-rab5a*, *nat*^{R}	This study
pERRFP	P*otef-cal*^{s}*-mrfp*-HDEL, *cbx*^{R}	(4)

a, *b*, mating-type loci; P, promoter; -, fusion; *hyg*^{R}, hygromycin resistance; *ble*^{R}, phleomycin resistance; *nat*^{R}, nourseothricin resistance; *cbx*^{R}, carboxin resistance; ^{ts}, temperature-sensitive allele; Δ, deletion; *I*, ectopically integrated; *crg*, conditional arabinose-induced promoter; *otef*, constitutive promoter; *nar*, conditional nitrate reductase promoter; *E1*, *W2*, genes of the *b* mating-type locus; NLS, nuclear localization signal of the GAL-4 DNA binding domain from pC-ACT1 (Clontech); *nup107*, nucleoporin; HDEL, ER retention signal; *egfp*, enhanced green fluorescent protein; *pagfp*, photoactivatable monomeric green fluorescent protein; *mrfp*, monomeric red fluorescent protein; *mcherry*, monomeric cherry; *dyn2*, C-terminal half of the dynein heavy chain; *rab5a*, small endosomal Rab5-like GTPase; *kin3*, kinesin-3.

1. Schuchardt I, Assmann D, Thines E, Schuberth C, Steinberg G (2005) Myosin-V, Kinesin-1, and Kinesin-3 cooperate in hyphal growth of the fungus *Ustilago maydis*. *Mol Biol Cell* 16: 5191–5201.
2. Lenz JH, Schuchardt I, Straube A, Steinberg G (2006) A dynein loading zone for retrograde endosome motility at microtubule plus-ends. *EMBO J* 25:2275–2286.
3. Wedlich-Söldner R, Schulz I, Straube A, Steinberg G (2002) Dynein supports motility of endoplasmic reticulum in the fungus *Ustilago maydis*. *Mol Biol Cell* 13:965–977.
4. Theisen U, Straube A, Steinberg G (2008) Dynamic rearrangement of nucleoporins during fungal "open" mitosis. *Mol Biol Cell* 19:1230–1240.
5. Wedlich-Söldner R, Straube A, Friedrich MW, Steinberg G (2002) A balance of KIF1A-like kinesin and dynein organizes early endosomes in the fungus *Ustilago maydis*. *EMBO J* 21: 2946–2957.

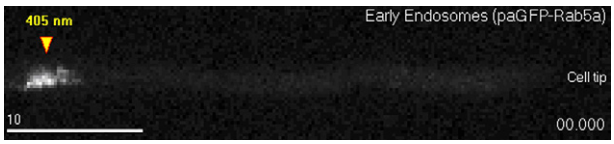

Movie S1. Anterograde motility of photoactivatable endosomal Rab5a. A single photoactivatable GFP was fused to the N terminus of the endosomal *rab5a* gene. After activation in the cell center using a 405-nm laser pulse (arrowheads), the anterogradely moving EEs become visible. Time is given in seconds: milliseconds. (Scale bar, 10 μm.)

Movie S1

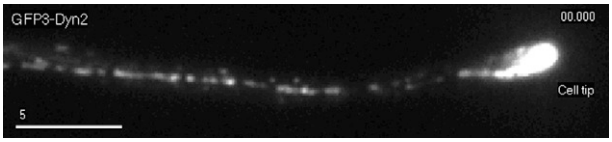

Movie S2. Motility of GFP$_3$-labeled dynein heavy chain. A triple-GFP tag was fused to the N terminus of the endogenous dynein heavy gene *dyn2*. The fusion protein displays bidirectional motility and concentrates at the microtubule plus ends near the hyphal tip. Time is given in seconds:milliseconds. (Scale bar, 5 μm.)

Movie S2

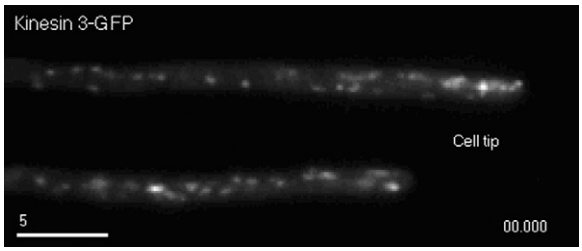

Movie S3. Motility of kinesin-3 fused to GFP. A GFP tag was fused to the C terminus of *kin3*, the kinesin-3 in *U. maydis*. The fusion protein displays long-range motility. Time is given in seconds:milliseconds. (Scale bar, 5 μm.)

Movie S3

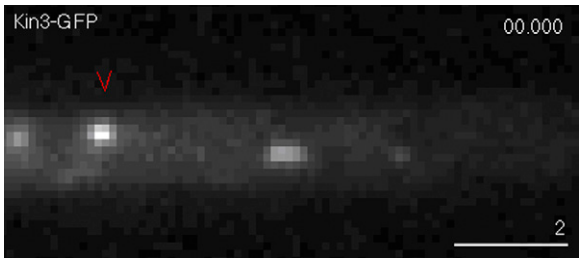

Movie S4. Bidirectional Kin3-GFP motility. A GFP tag was fused to the C terminus of *kin3*, the kinesin-3 in *U. maydis*. Single signals show processive and bidirectional motility (red arrowhead). Time is given in seconds:milliseconds. (Scale bar, 2 μm.)

Movie S4

Movie S5. Colocalization of kinesin-3 and early endosomes. Kin3-GFP (green) was coexpressed with mCherry-Rab5a (red). The hypha was partially photobleached to visualize only the anterograde transport. Time is given in seconds:milliseconds. (Scale bar, 3 μm.)

Movie S5

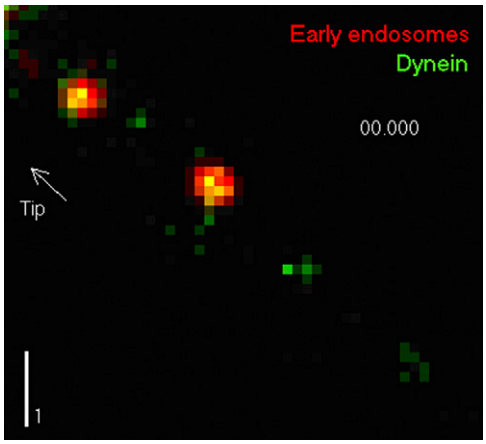

Movie S6. Colocalization of dynein and early endosomes. Retrograde EEs (marked by mCherry-Rab5a, red) colocalize with dynein (labeled by GFP_3-Dyn2). Note that red signals move in an anterograde direction to the tip, which is mediated by kinesin-3. Time is given in seconds:milliseconds. (Scale bar, 1 μm.)

Movie S6

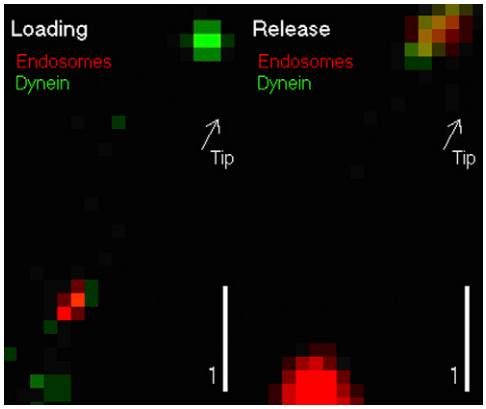

Movie S7. "On-the-run" loading and release of EE and dynein. Loading: Anterograde EE (marked by mCherry-Rab5a, red) meets a retrograde dynein (labeled by GFP_3-Dyn2, green). The dynein binds to the EE and changes the transport direction. Release: Dynein and EEs colocalize while moving in a retrograde direction. An EE (red) moves in an anterograde direction to the tip, which is mediated by kinesin-3. Time is given in seconds:milliseconds. (Scale bars, 1 μm.)

Movie S7

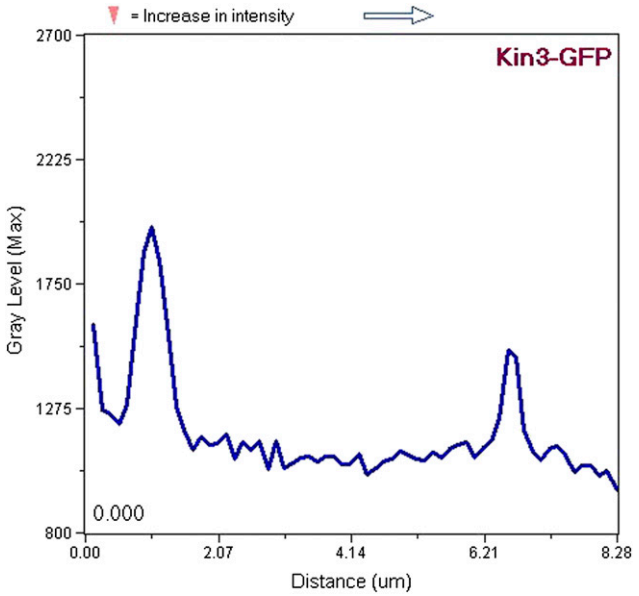

Movie S8. Fluctuation of Kinesin-3–GFP intensities during bidirectional motility. A series of graphs shows intensity line scans over moving kinesin-3–GFP. Increases in signal intensities are indicated by red arrowheads at the top of the graph. Note that intensity increase occurs randomly along the track, showing that it is not due to the track leaving the focal plane. Time in seconds:milliseconds is shown in the lower left near the axis origin. The arrow at the top indicates direction to the cell tip (right).

Movie S8